processes

MDPI

Article

Mechanism of Surface Wettability of Nanostructure Morphology Enhancing Boiling Heat Transfer: Molecular Dynamics Simulation

Wenting Guo [1,2], Liangcai Zeng [2,3,*] and Zhuoyuan Liu [1,3]

[1] Key Laboratory of Metallurgical Equipment and Control Technology, Ministry of Education, Wuhan University of Science and Technology, Wuhan 430081, China
[2] Hubei Key Laboratory of Mechanical Transmission and Manufacturing Engineering, Wuhan University of Science and Technology, Wuhan 430081, China
[3] Precision Manufacturing Institute, Wuhan University of Science and Technology, Wuhan 430081, China
* Correspondence: zengliangcai@wust.edu.cn

Abstract: In this paper, the interaction mechanism between the solid–liquid–gas interface phenomenon caused by nanostructure and surface wettability and boiling heat transfer is described, and the heat transfer theory of single wettable nanostructure surface and mixed wettable nanostructure surface is proposed. Through molecular dynamics simulation, the thermodynamic model of the wettable surface of nanostructures is established. The nanostructures are set as four rectangular lattice structures with a height of 18 Å. The solid atoms are platinum atoms, and the liquid atoms are argon atoms. The simulation results show that with the increase of surface hydrophilicity of nanostructures, the fluid temperature increases significantly, and the heat transfer at the interface is enhanced. With the increase in surface hydrophobicity of nanostructures, the atoms staying on the surface of nanostructures are affected by the hydrophobicity, showing a phenomenon of exclusion, and the evaporation rate in the evaporation area of nanostructures is significantly increased. In addition, the mixed wettable surface is influenced by the atomic potential energy and kinetic energy of the solid surface, and when compared with the pure wettable surface under the nanostructure, it changes the diffusion behavior of argon atoms on the nanostructure surface, enhances the heat transfer phenomenon compared with the pure hydrophobic surface, and enhances the evaporation phenomenon compared with the pure hydrophilic surface. This study provides insights into the relationship between the vapor film and the heating surface with mixed wettability and nanostructures.

Keywords: boiling heat transfer; nanostructure; kinetic energy; potential energy; wettability

Citation: Guo, W.; Zeng, L.; Liu, Z. Mechanism of Surface Wettability of Nanostructure Morphology Enhancing Boiling Heat Transfer: Molecular Dynamics Simulation. *Processes* **2023**, *11*, 857. https://doi.org/10.3390/pr11030857

Academic Editor: Blaž Likozar

Received: 20 February 2023
Revised: 8 March 2023
Accepted: 8 March 2023
Published: 13 March 2023

1. Introduction

The field of microelectronics has undergone significant advancements in recent years due to rapid technological progress; the integration of electronic devices has jumped at a rate of 40–50% every year, and the scale of micro/nanodevices tends to microns and nanometers. As the surface area to volume ratio has increased, the influence of various interface characteristics and surface forces on devices has become dominant [1]. Among them, temperature is one of the main causes of mechanical negative effects in the traditional sense. In the microsystems, its interface effect is more sensitive to the friction heat and working condition temperature in the movement process. Furthermore, the process of converting liquid into gas through a heated surface involves a temperature-driven mechanism whereby thermal energy is transferred to the liquid, leading to its vaporization. This transformation is facilitated by the movement of liquid through buoyancy, which acts as a carrier for the resulting vapor. This phenomenon is called the Leidenfrost liquid suspension effect and is caused by boiling heat transfer [2–4], which makes the temperature as the nanobubbles intervene in the solid–liquid interface medium. At the same time, the

resistance produced by gas in the friction process of micro-nanodevices is far less than that of liquid, thus successfully converting the negative thermal effects into available energy resources [4–6].

When the contact angle of the droplet is close to 0, the hydrophilic surface shows spontaneous diffusion [7,8]. When the liquid contact angle is greater than 150°, the surface is called a superhydrophobic surface, which has an obvious high contact angle and contact angle hysteresis, providing the self-cleaning ability of the surface, enabling the gas to stay on the surface and reducing the fluid flow resistance [9]. Extensive research has shown that surface wettability and nanostructure play a crucial role in boiling evaporation heat transfer [10]. The number of vaporization cores, growth and growth processes, temperature and pressure changes in phase transformation, and energy conversion caused by phase transformation in the explosive boiling process are key problems for industrial applications. Rapid heating of liquid working substances, such as bubble column isobaric heating technology and capillary isobaric heating technology, can reduce the requirements for impurities, dissolved gases, surface cleanliness, etc. In addition, the application of laser heat sources with nanoscale electric pulse heating and laser pulse heating has opened up new engineering and technical applications. However, up to now, with the continuous development of micro-nanoelectronic devices, traditional thermodynamic theory is not applicable to the micro-state. Compared with the difficulties of experimental research, by resolving the molecule/atomic interaction force, the invention of the molecular dynamics approach offers a way to watch and investigate the phase change process at the nanoscale, which has been extensively acknowledged and used [11,12]. Wang et al. simulated the process of liquid film evaporation and explosive boiling on a single wettable surface through molecular dynamics, focusing on the superheat and Kapitza thermal resistance differences that trigger explosive boiling under different liquid film thicknesses. The concept of critical thickness explains the controversial issues between nanoexplosive boiling and classical nucleation theory and has a better theoretical understanding at the microscopic level [13]. Zhou et al. studied the bubble nucleation process of liquid argon on different wettability surfaces by using MD simulation, noticed the dynamic bubble behavior and bubble nucleation position at various wall temperatures., discussed the interface differences between solid–liquid–gas on different wetted surfaces, and they discovered that bubble nucleation frequently took place in the wall's hydrophobic region at low wall temperatures and that as wall temperature increased, the bubble location progressively shifted from the hydrophobic zone to the hydrophilic zone [14]. Diaz et al., respectively, studied the difference between surface wettability and surface structure in terms of heat flux. Hydrophilic surfaces and hydrophilic structures may promote boiling and have the maximum heat flux, as demonstrated by the slow rise in overheating that eventually led to the onset of nucleate boiling and the transfer of the critical heat flux (CHF) to the membrane boiling state [15]. Focusing on the first step of nucleation boiling, Zhang et al. examined the behavior of liquid film bubbles on smooth surfaces vs nanostructured surfaces, and discovered that nanostructured surfaces are favorable to local bubble nucleation and may considerably increase nucleation boiling [16]. Through MD, Seyf et al. investigated the impact of several nanomaterials (including silver and aluminum) on the explosive boiling of liquid argon film on the nanostructure. The findings demonstrated that the conical nanostructure, mostly because of its size, considerably improved the heat transfer efficiency between solid and liquid but had no impact on the material [17]. Fu et al. compared the phase transition process of nanostructured copper plates at three different heights with that in the plane during rapid boiling, and the findings demonstrated that when the height of nanostructures rose, the liquid's equilibrium temperature on the surface of high-temperature copper plates also increased [18,19]. Zhao et al. studied the bubble nucleation and heat transfer performance of groove surfaces with different wettability, compared the differences of three-phase contact lines on different groove surfaces, and provided insights for the nucleation of nanobubbles on the structural surface [20]. In order to explain how bubble nuclei develop on various wetted substrates, Chen et al. used a

model based on the conflict between atomic potential energy and atomic kinetic energy. The findings demonstrated that the grooves significantly influenced bubble nucleation in two ways: by increasing the effectiveness of heat transmission and by sustaining the first bubble nucleus [21]. Jo et al. studied the boiling wetting phenomenon of hydrophilic and hydrophobic surfaces without microscale roughness. Based on the bubble analysis results, when the microstructure does not exist, the stable change of wettability will lead to completely different boiling states. In addition, at low heat flux, hydrophobic surfaces provide better nucleate boiling than hydrophilic surfaces [22,23]. Wang et al. established a molecular dynamics model of subcooled boiling of copper plate, liquid water, and gaseous water and discussed the nanobubbles' generation and condensation process under different wall superheat temperatures. The simulation structure shows that with the increase of wall superheat, the nanobubbles become rich and the condensation behavior becomes more rapid. This process tends to converge horizontally on the flat copper plate surface. On the contrary, on the surface of nanostructures, the nanostructured cavities are more likely to induce condensation to incline to vertical convection [24]. Based on different materials and manufacturing methods, Li et al. discussed the difference in critical heat flux and heat transfer coefficient between different micro and nanostructure morphologies. The research shows that the structure gap or porous material pore in the nanostructure is easy to cause obvious negative pressure, which provides an additional heat and mass transfer mechanism [25]. Wu et al. established the pool boiling model of copper plate and water, showing the distribution and proportion of different wettability by adjusting the smooth copper plate, and discussing the boiling heat transfer process of different wettability [26]. Cao [27] et al. focused on the change between liquid and gas, and pointed out that in the molecular dynamics simulation of rapid boiling of the copper substrate and argon liquid, when the thickness of argon liquid was far greater than 1 nm, the wettability had no significant effect on the change of gas–liquid interface. Liang [28] et al., studied the evaporation and condensation process of fluid in the microchannel by molecular dynamics method, and discussed the heat transfer process between the evaporation surface and the condensation surface of the microchannel by changing the substrate temperature in both instantaneous and periodic ways. The accuracy of the model is confirmed, and it is shown that the evaporation and condensation process is mainly through diffusion rather than convection.

Recent research has shown that wettability and nanostructure are favorable for the formation of nanobubbles and improved heat transmission [29–31]. A large number of studies have focused on pure wettable surfaces or single structural surfaces to reveal the impact on boiling heat transfer efficiency and surface bubble nucleation, while less consideration has been given to the coupling effect of mixed wettability surfaces and mixed structural surfaces. Research on the impact of surface on boiling heat transfer has gotten more complicated recently due to the rise in coupled surface features. At present, the influence of the coupling of nanostructure and mixed wettability on bubble nucleation and enhanced heat transfer is not clear. At the same time, the change of vapor film caused by the gas–liquid phase transition in the boiling process was ignored.

In this study, the difference between the coupling effect of nanostructure and mixed wettability on the temperature response of heated surface liquid is focused. Based on the method of molecular dynamics, a surface model with a rectangular lattice is established. At the same time, four different wettability (pure hydrophilic, pure hydrophobic, and two mixed wetted) are given to the nanostructure surface. The pool boiling phenomenon in the model is observed, and the heat transfer efficiency of solid–liquid–gas three-phase is analyzed. According to the motion state of liquid mass, the nucleation phenomenon of nanobubbles is judged. The molecular motion state under four surfaces is visually tested through the complete boiling evaporation process. The atomic potential energy and atomic kinetic energy explain the differences between different nanostructures and wettable surfaces. The thermal mechanism of the coupling effect of nanostructure and mixed wettability under explosive boiling was explored at the nanoscale.

2. Models and Methods

In order to more intuitively describe the physical state of molecules under boiling heat transfer, a 80 Å(x) × 80 Å(y) × 300 Å(z) simulation box was created, as shown in Figure 1. The simulation box comprises solid, liquid, and gas phases, with the liquid and gas phases consisting of argon atoms (in blue), and lattice constants of 5.77 Å and 32.87 Å, respectively. According to the arrangement rule of face-centered cubic (FCC; 111), the liquid atoms are distributed above the solid surface, and the gas atoms are distributed above the liquid atoms, which together constitute the gas–liquid environment of the whole boiling model. The solid atoms are platinum atoms, which are arranged according to face-centered cubic (FCC; 111) to form different structures with a lattice constant of 3.92 Å, as shown in Figure 1b. In order to restore the physical structure of the metal heating surface more realistically, the solid platinum surface is set as a three-layer atomic arrangement structure, the bottom Fixedlayers (purple) wall samples migrate and deform, and the Heatsource (green) in the middle layer is the heat source that generates heat flux, the upper layer is the Reallayers (red for hydrophilic and yellow for hydrophobic) through which heat is conducted to the argon fluid.

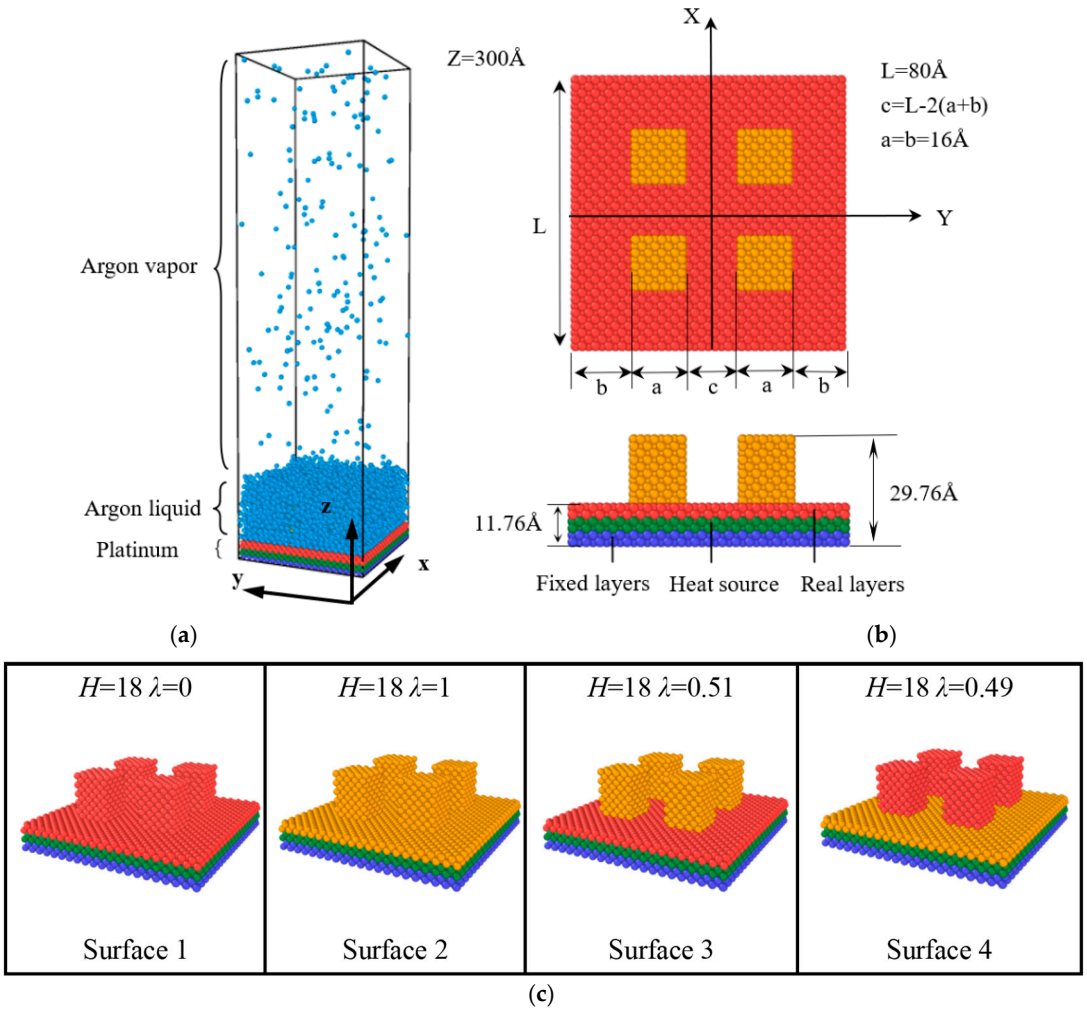

Figure 1. Boiling heat transfer models of different nanostructured wetted surfaces, (**a**) three-dimensional view of surface 3, (**b**) dimensional schematic diagram of surface 3, and (**c**) schematic diagram of four surfaces.

In order to analyze the coupling effect of different wetting methods on boiling heat transfer under nanostructures and endow nanostructures with different hydrophilic–

hydrophobic wetting characteristics, four different surface structures were designed, as shown in Figure 1c. The four surfaces have nanostructures. The height of the nanostructure is set as H (Å), and surface 1 is a pure hydrophilic nanostructure surface. Surface 2 is a pure hydrophobic nanostructure surface. Surface 3 is a mixed wettability nanostructure surface, the substrate surface is hydrophilic, and the nanostructure is hydrophobic. Surface 4 is also a mixed wettability nanostructure surface, the substrate surface is hydrophobic, and the nanostructure is hydrophilic. In order to distinguish these four surfaces more intuitively, the wetting ratio (λ), namely the ratio of hydrophobic nanosurface area to the total contact area, is proposed. It is worth pointing out that the nanostructures on the surface 1–4 are three-dimensional square matrix structures, showing regular arrangement. The width of nanostructures is equal to the spacing of nanostructures. In addition, surfaces 1–4 are also a square structure; in other words, in the X direction and the Y direction, the nanostructure surface has the same view and value. According to the values given in Figure 1b, the wetting ratio of the four surfaces can be obtained by calculating the contact area of the wetted surface, where λ is 0, 1, 0.51, and 0.49, respectively.

To prevent atom loss, a specular reflection is set on the top of the simulation box, and periodic boundary conditions are set in the X and Y axes directions, so there is no loss of energy and momentum, only the exchange between atoms. As the most famous interaction potential in MD simulation, Lennard Jones (LJ) interaction potential is often used to describe the interaction between gas and liquid molecules. Previous research work shows that LJ potential can make a relatively accurate description of argon atom pairs [12,21], which is described as follows:

$$\varphi_{Ar\text{-}Ar}(r) = 4\varepsilon_{Ar\text{-}Ar}\left[\left(\frac{\sigma_{Ar\text{-}Ar}}{r}\right)^{12} - \left(\frac{\sigma_{Ar\text{-}Ar}}{r}\right)^{6}\right] \quad (1)$$

$$\varphi_{Pt\text{-}Pt}(r) = 4\varepsilon_{Pt\text{-}Pt}\left[\left(\frac{\sigma_{Pt\text{-}Pt}}{r}\right)^{12} - \left(\frac{\sigma_{Pt\text{-}Pt}}{r}\right)^{6}\right] \quad (2)$$

where ε and σ express the interaction strength and the interaction radius. The interaction between argon platinum atom pairs is related to the wettability of the solid–liquid interface. In order to accurately reduce the hydrophilic–hydrophobic wetting characteristics in the model, a new Lorentz Berthelot combining rule is adopted, as shown in the equation:

$$\varphi_{Ar\text{-}Pt}(r) = 4c\varepsilon_{Ar\text{-}Pt}\left[\left(\frac{\sigma_{Ar\text{-}Pt}}{r}\right)^{12} - \left(\frac{\sigma_{Ar\text{-}Pt}}{r}\right)^{6}\right] \quad (3)$$

where the cutoff distance of the potential function is set at $r = 4\sigma_{Ar\text{-}Ar} = 13.62$ Å, and c is detailed in Table 1 as the potential energy coefficient to adjust the surface wettability. The contact angle is usually pointed out to characterize the wetting characteristics of the surface. In this study, the contact angle of the hydrophilic surface (red) is 65°, and that of the hydrophobic surface (yellow) is 113°.

Table 1. Values of various LJ parameters.

Molecules	ε (eV)	σ (Å)
Argon–Argon (Ar–Ar)	0.010438	3.405
Argon–Platinum (hydrophilic, c = 1) (Ar–Pt)	0.060486	2.990
Argon–Platinum (hydrophobic, c = 0.66) (Ar–Pt)	0.004175	2.990
Platinum–Platinum (Pt–Pt)	0.351	2.574

The velocity Verlet algorithm was used to solve the nanoparticle motion equation. This calculating in the following way [32]:

$$r(t + \Delta t) = r(t) + v(t)\Delta t + \frac{1}{2m}F(t)\Delta t^2 \quad (4)$$

$$v(t+\Delta t) = v(t) + \frac{1}{2m}[F(t) + F(t+\Delta t)]\Delta t \quad (5)$$

where t is the integration time step, at any given time t, the position vector, velocity vector, and acceleration vector of an atom are represented by $r(t)$, $v(t)$, and $F(t)$, respectively. The time step used in this study is Δt = 0.001 ps, and it is used to update the particle locations and velocities.

The whole simulation was divided into two stages. First, the whole domain was always maintained in the micro canonical (NVT) ensemble (constant number of atoms, constant volume and constant temperature). A Langevin thermostat was used to adjust the temperature of argon atoms. The two layers above the platinum wall (hot layer and real layer) used the velocity rescaling method to control the temperature of the whole system to be kept at 90 K to achieve thermal equilibrium. The whole process lasted for 0.3 ns. In the second stage, in order to more accurately reduce the heat transfer process of solid, liquid, and gas, the temperature control of liquid and gas was carried out after relaxation, but only for the heat source layer. At the same time, the temperature input of the heat source layer was changed, giving a significant temperature rise to the whole boiling model, and the temperature rose from 90 K to 298 K after relaxation. We then kept, observed and counted the atomic motion law and thermodynamic transfer in this state. The data collection was once every 100 ps until the end of the simulation. The process lasted for 3 ns. All simulation processes were completed by open-source code lammps simulation, and system visualization was completed by ovito.

3. Results and Discussion

3.1. Movement and Distribution of Argon Atoms

Four different nanostructure wetted surfaces S1, S2, S3, and S4 were simulated to better understand the influence of the coupling effect of the nanostructure and mixed wettability on enhanced boiling heat transfer under different conditions, which represent pure hydrophilic textured surfaces (H = 18, λ = 0), pure hydrophobic structure surfaces (H = 18, λ = 1), hydrophilic substrates and hydrophobic nanostructures (H = 18, λ = 0.51), as well as hydrophobic bottoms and hydrophilic nanostructures (H = 18, λ = 0.49), respectively. Figure 2 shows the boiling of argon atoms on four surfaces and the distribution of vapor film movement at 298 K. As shown in Figure 2, in the initial state, the liquid layer completely covered the wetted surface of the nanostructure. With the occurrence of boiling heat transfer, the liquid atoms were affected by temperature, overcoming the influence of surface interaction, and began to diffuse. They experienced four stages: natural convection, nuclear boiling, transition boiling, and stable membrane boiling. The bubbles gradually fuse and expand until the solid–liquid two phases are completely separated. The whole simulation region is now separated into three sections: the liquid layer floating above, the middle vapor layer, and the adsorbed liquid layer on the top of the nanostructure. Observing the vapor layer indicated by the red circle in the figure, it can be found that the liquid layer rises rapidly when the pure hydrophilic surface is 0.2 ns, but due to the influence of the hydrophilic texture surface, argon atoms are deposited on the textured surface in a large area, and the number of rising liquid atoms was less visible than other surfaces; At 0.8 ns, the liquid layer on the pure hydrophobic surface increased significantly; on surface 3 (λ = 0.51), an obvious argon vapor layer appears at 0.2 ns. At this time, the hydrophilic bottom was covered with a thin layer of argon atoms, and the number of argon atoms around the hydrophobic texture was small; on surface 4 (λ = 0.49), the rise of the liquid layer occurred at 0.3 ns. At this time, a large number of atoms were accumulated on the textured surface, and the vapor layer was not obvious.

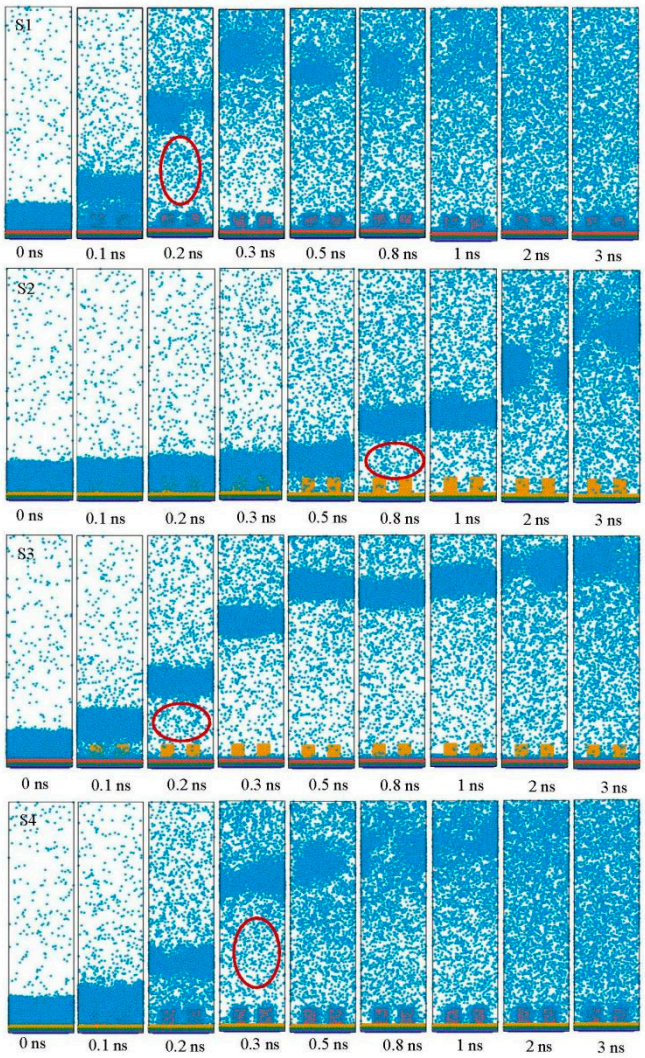

Figure 2. Snapshot of rapid boiling process on surfaces 1–4.

3.2. Surface Dynamics Analysis and Nucleation of Nanostructures

In order to more accurately describe the coupling effect of different nanostructure wetted surfaces on argon atoms, Figure 3 shows the changing trend of kinetic energy, potential energy and x-axis density of argon atoms on the nanostructure surface in the evaporation region of 10 Å above the wall at 1 ns. Kinetic energy (Ke) refers to the ability of argon atoms to move due to interaction on the wetted surface. The higher the speed, the greater its kinetic energy. Potential energy (Pe) refers to the energy generated by the interaction between molecules, which is divided into repulsion force and attraction force. The stronger the hydrophilicity is, the greater the absolute value of the surface potential energy is. As shown in Figure 3a,d, the potential energy values on the pure hydrophilic surface 1 and the mixed wetted surface 4 are -0.2 ev and -0.16 ev, respectively. The Pe values of these two surfaces are similar in the whole surface area. Interestingly, the argon atom density and potential energy on the nanochannels of the pure hydrophilic surface 1 show an obvious symmetrical opposite trend (marked by the green box in the figure). As shown in Figure 3b,c, the potential energy value on the pure hydrophobic surface 2 and the mixed wetted surface 3 tends to be close to 0, and the attraction to atoms is smaller, so that the surface hydrophobicity is a reasonable explanation for describing this phenomenon. In addition, the argon atom density in the hydrophobic region is significantly lower than that in the hydrophilic region. It is worth pointing out that under the action of nanostructures, the two wettability surfaces are limited by surface pits, showing different nucleation states.

The hydrophilic surface is covered with an adsorbed liquid layer, and the nucleation of nanobubbles is in the center of the pit. The bubble nucleation on the hydrophobic surface is on the wall, and there are more bubble nucleation points. The adsorption liquid layer and gas nucleation point under the mixed wetting surface appeared at the same time.

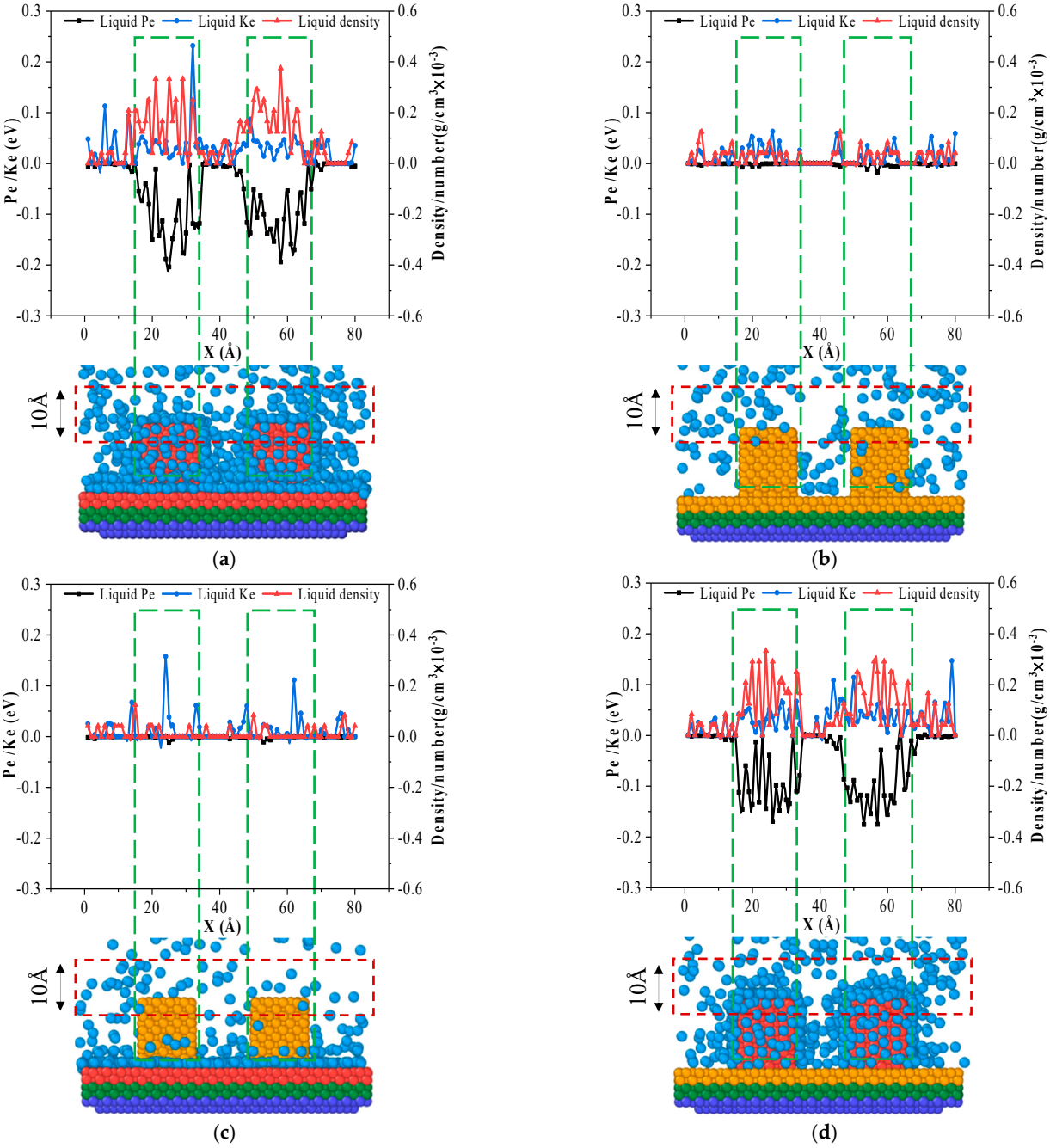

Figure 3. Kinetic energy, potential energy, and x-axis density of argon atoms in the evaporation zone of the surfaces, (**a**) surface 1, (**b**) surface 2, (**c**) surface 3, (**d**) surface 4.

3.3. Thermodynamic Analysis

Figure 4 shows the temperature changes of platinum and argon atoms on the wetted surface of nanostructures during boiling. As shown in Figure 4a, when the temperature of the heat source layer changes, the upper platinum atoms respond quickly to the temperature change, reach the target temperature of 298 K stably within 0.1 ns and float up and down in a small range, which is precisely due to the continuous heat transfer between the platinum

surface and argon atoms. As shown in Figure 4b, the temperature change of argon atoms after boiling heat transfer is described. Affected by the wall heat source, argon atoms receive temperature transfer from the heat source from the wetted surface, which conforms to the typical boiling heat transfer curve. The black, red, blue, and green arrows point out the time and temperature changes when surface 1–4 explosive boiling occurs. At this time, large-scale gas–liquid phase transition begins to occur. An obvious feature is that the liquid atoms evaporate into clusters and separate from the wall, the gas layer replaces the liquid to fill the nanostructured surface, and the temperature rise process of argon atoms begins to slow down. The reason for this phenomenon is that the heat transfer effect of gas is far lower than that of liquid. In order to compare the heat transfer differences of different wettable surfaces under nanostructures, the wall superheat (ΔT) is defined, which represents the difference between the heated wall temperature and the explosive boiling temperature of the liquid, surface 1 (H = 18, λ = 0) explosive boiling begins at 0.22 ns, when the liquid temperature is 204 k and the wall superheat ΔT1 = 94 K. ΔT2 = 165 K, ΔT3 = 142 K, ΔT4 = 114 K represent surface 2, surface 3, and surface 4 respectively. For four surfaces, the value of ΔT increases with a decrease in ratio (λ). In other words, the hydrophilic surface provides more favorable conditions for the explosive boiling of nanofilms than the hydrophobic surface.

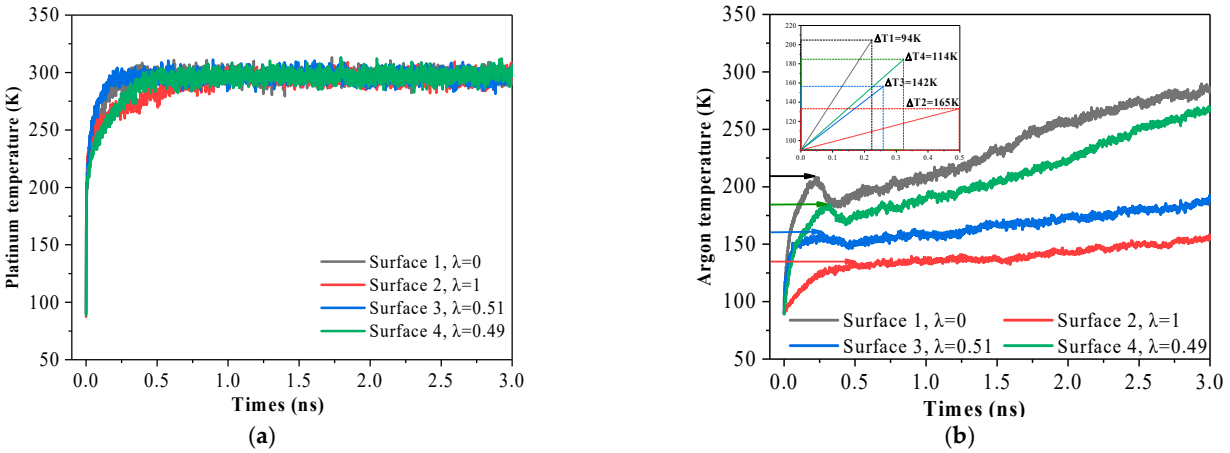

Figure 4. Temperature changes of platinum and argon atoms on the nanostructured wetted surface under 298 K temperature input: (**a**) platinum atom (**b**) argon atom.

3.4. Evaporation Rate of Nanostructure Wetted Surface

Figure 5a–d shows the numerical density changes of the liquid layer in the z-axis of the surfaces in the time periods of 0 ns, 0.1 ns, 0.2 ns, 0.3 ns, 0.5 ns, 1 ns, 2 ns, and 3 ns. The simulation results show that the density change of the liquid layer above the heated nanosurface shows a consistent change law. With the increase in temperature, a large number of liquid layers evaporate and converge into small clusters, and the maximum value of the numerical density decreases rapidly and moves up the z-axis. For the pure hydrophilic nanostructure surface, more heat is transferred to the structure surface to produce a gas–liquid phase transition. The maximum value decreases by 50% at 0.1 ns, and the liquid layer reaches its highest point at 0.3 ns. For the surface of pure hydrophobic nanostructures, the maximum value of the number density changes more gently. In order to more accurately analyze the evaporation phenomenon of the liquid layer on different wetted surfaces, the area of 10 Å above the nanostructure is defined as the wall evaporation area (described by the red dotted box). According to the numerical density value given in Figure 5, the evaporation rate is defined as the ratio of the number of argon atoms in the evaporation region at each moment to the initial number of atoms in the evaporation region. The specific value is given in Figure 6. In all cases, the evaporation rate of liquid atoms on the surface of nanostructures increases significantly with the increase in temperature. The

maximum evaporation rate of surface 1 (H = 18, λ = 0) at 0.28 ns was 90.2%; on Surface 2 (H = 18, λ = 1), the maximum evaporation rate was 96.3% at 1.53 ns; on surface 3, (H = 18, λ = 0.51) of the maximum evaporation rate is 98% at 0.31 ns; on Surface 4, (H = 18, λ = 0.49) reached the maximum evaporation rate of 88.5% at 0.38 ns. It is worth noting that the argon atom evaporation rate of the pure hydrophobic surface was significantly higher than that of the pure hydrophilic surface. For the mixed wetted surface with λ = 0.51, the time to reach the maximum evaporation rate was only 1/5 of surface 2, and the maximum evaporation rate was 13.7% higher than surface 1.

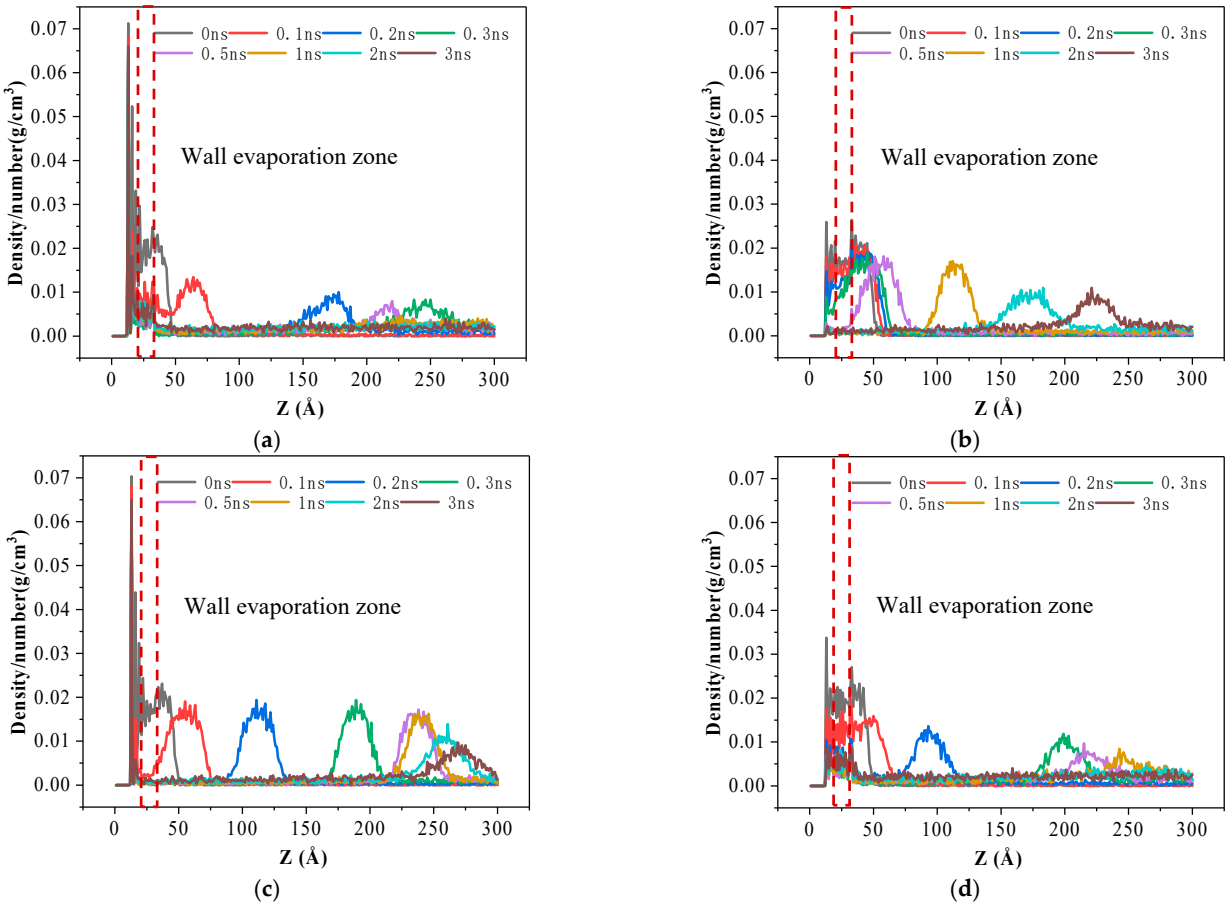

Figure 5. Number density changes of four surfaces at different times: (**a**) surface 1, (**b**) surface 2, (**c**) surface 3, and (**d**) surface 4.

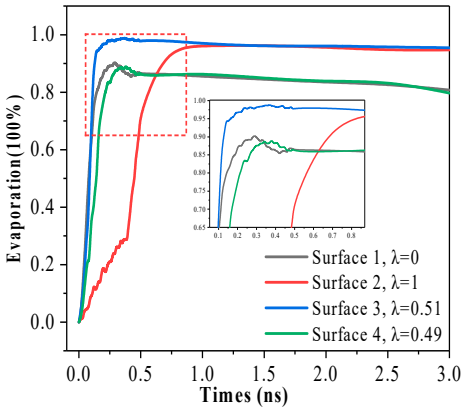

Figure 6. Evaporation rate of surface 1–4, the maximum evaporation rate of surfaces 1–4 is 90.2%, 96.3%, 98%, and 88.5%, respectively.

4. Conclusions

The main objective of this study is to investigate the thermal theory behind solid–liquid–gas interface phenomenon that occurs on heated surfaces with nanostructures and wettability. The study uses molecular dynamics simulation to explore how surfaces with different nanostructures affect boiling evaporation heat transfer and to evaluate and compare the phase transition processes of argon vapor films on four different wetted nanostructures. The study also examines surface dynamics, heat transfer characteristics, and evaporation rate. The key findings of the study are summarized as follows:

1. The pure hydrophilic nanostructure surface requires a significantly lower surface superheat for the gas–liquid phase transition to become evident compared to the pure hydrophobic nanostructure surface. It is worth pointing out that the hydrophilic surface responds quickly to the temperature change; the fluid temperature rises rapidly, reaches the critical point of gas–liquid phase change faster, and enhances the heat transfer.
2. Due to the increase of surface hydrophobicity, the atoms staying on the solid surface are affected by kinetic energy and potential energy, showing a repulsion phenomenon. The change of atomic number density in the evaporation area of the solid surface is called the evaporation rate. The change in evaporation rate confirmed that the force of pure hydrophobic nanostructure surface on argon atoms was weak, so more argon atoms diffused from the surface, and the evaporation rate was significantly improved.
3. Further research shows that the capillary transmission is enhanced on the mixed wettability nanostructure surface, and the wettability is limited by the surface pits. The efficiency of three-phase heat transmission between solid, liquid, and gas is improved when compared to pure hydrophobic surfaces, and when compared to pure hydrophilic surfaces, the rate of evaporation and the formation of nanobubbles are encouraged.

Author Contributions: Conceptualization, W.G. and Z.L.; methodology, L.Z.; software, W.G.; validation, W.G., Z.L. and L.Z.; formal analysis, W.G.; investigation, W.G.; resources, L.Z.; data curation, W.G.; writing—original draft preparation, W.G.; writing—review and editing, Z.L.; visualization, L.Z.; supervision, L.Z. All authors have read and agreed to the published version of the manuscript.

Funding: This work was financially supported by the National Natural Science Foundation of China (Grant Nos. 51975425), and the Natural Science Foundation of Hubei Province, China, (Grant Nos. 2022CFB603).

Acknowledgments: The authors gratefully acknowledge these supports.

Conflicts of Interest: The authors declare no conflict of interest.

References

1. Verlag, S. *Springer Handbook of Nanotechnology*; Harbin Institute of Technology Press: Harbin, China, 2013.
2. Carey, V.P. Molecular dynamics simulations and liquid-vapor phase-change phenomena. *Microscale Thermophys. Eng.* **2002**, *6*, 1–2. [CrossRef]
3. Ceccio, S.L. Friction Drag Reduction of External Flows with Bubble and Gas Injection. *Annu. Rev. Fluid Mech.* **2010**, *42*, 183–203. [CrossRef]
4. Rothstein, J.P. Slip on Superhydrophobic Surfaces. *Annu. Rev. Fluid Mech.* **2010**, *42*, 89–109. [CrossRef]
5. Elbing, B.R.; Winkel, E.S.; Lay, K.A.; Ceccio, S.L.; Dowling, D.R.; Perlin, M. Bubble-induced skin-friction drag reduction and the abrupt transition to air-layer drag reduction. *J. Fluid Mech.* **2008**, *612*, 201–236. [CrossRef]
6. Elbing, B.R.; Mkiharju, S.; Wiggins, A.; Perlin, M.; Dowling, D.R.; Ceccio, S.L. On the scaling of air layer drag reduction. *J. Fluid Mech.* **2013**, *717*, 484–513. [CrossRef]
7. Bhushan, B.; Jung, Y.C. Natural and biomimetic artificial surfaces for superhydrophobicity, self-cleaning, low adhesion, and drag reduction. *Prog. Mater. Sci.* **2011**, *56*, 1–108. [CrossRef]
8. Nosonovsky, M. Materials science: Slippery when wetted. *Nature* **2011**, *477*, 412–413. [CrossRef]
9. Betz, A.R.; Jenkins, J.; Kim, C.-J.; Attinger, D. Boiling heat transfer on superhydrophilic, superhydrophobic, and superbiphilic surfaces. *Int. J. Heat Mass Transf.* **2013**, *57*, 733–741. [CrossRef]

10. Liang, G.; Mudawar, I. Review of pool boiling enhancement by surface modification. *Int. J. Heat Mass Transf.* **2019**, *128*, 892–933. [CrossRef]
11. Kim, J. Review of nucleate pool boiling bubble heat transfer mechanisms. *Int. J. Multiph. Flow* **2009**, *35*, 1067–1076. [CrossRef]
12. Lu, Y. Molecular-continuum simulation of elevated temperature drag reduction by nanostructure-induced vapor layer. *Int. J. Heat Mass Transf.* **2019**, *148*, 119100. [CrossRef]
13. Wang, Y.H.; Wang, S.Y.; Lu, G.; Wang, X.-D. Effects of wettability on explosive boiling of nanoscale liquid films: Whether the classical nucleation theory fails or not? *Int. J. Heat Mass Transf.* **2019**, *132*, 1277–1283. [CrossRef]
14. Zhou, W.; Li, Y.; Li, M.; Wei, J.; Tao, W. Bubble nucleation over patterned surfaces with different wettabilities: Molecular dynamics investigation. *Int. J. Heat Mass Transf.* **2019**, *136*, 1–9. [CrossRef]
15. Diaz, R.; Guo, Z. Molecular dynamics study of wettability and pitch effects on maximum critical heat flux in evaporation and pool boiling heat transfer. *Numer. Heat Transf. Part A Appl.* **2017**, *72*, 891–903. [CrossRef]
16. Zhang, L.; Xu, J.; Liu, G.; Lei, J. Nucleate boiling on nanostructured surfaces using molecular dynamics simulations. *Int. J. Therm. Sci.* **2020**, *152*, 106325. [CrossRef]
17. Seyf, H.R.; Zhang, Y. Effect of nanotextured array of conical features on explosive boiling over a flat substrate: A nonequilibrium molecular dynamics study. *Int. J. Heat Mass Transf.* **2013**, *66*, 613–624. [CrossRef]
18. Fu, T.; Mao, Y.; Tang, Y.; Zhang, Y.; Yuan, W. Effect of nanostructure on rapid boiling of water on a hot copper plate: A molecular dynamics study. *Heat Mass Transf.* **2016**, *52*, 1469–1478. [CrossRef]
19. Fu, T.; Mao, Y.; Tang, Y.; Zhang, Y.; Yuan, Q. Molecular Dynamics Simulation on Rapid Boiling of Thin Water Films on Cone-Shaped Nanostructure Surfaces. *Nanoscale Microscale Thermophys. Eng.* **2015**, *19*, 17–30. [CrossRef]
20. Zhao, H.; Zhou, L.; Du, X. Bubble nucleation on grooved surfaces with hybrid wettability: Molecular dynamics study under a transient temperature boundary condition. *Int. J. Heat Mass Transf.* **2021**, *166*, 120752. [CrossRef]
21. Chen, Y.J.; Yu, B.; Zou, Y.; Chen, B.-N.; Tao, W.-Q. Molecular dynamics studies of bubble nucleation on a grooved substrate. *Int. J. Heat Mass Transf.* **2020**, *158*, 119850. [CrossRef]
22. Jo, H.J.; Ahn, H.S.; Kang, S.H.; Kim, M.H. A study of nucleate boiling heat transfer on hydrophilic, hydrophobic and heterogeneous wetting surfaces. *Int. J. Heat Mass Transf.* **2011**, *54*, 5643–5652. [CrossRef]
23. Bourdon, B.; Marco, P.D.; Rioboo, R.; Marengo, M.; De Coninck, J. Enhancing the onset of pool boiling by wettability modification on nanometrically smooth surfaces. *Int. Commun. Heat Mass Transf.* **2013**, *45*, 11–15. [CrossRef]
24. Wang, W.; Shenghong, H.; Xisheng, L. MD simulation on nano-scale heat transfer mechanism of sub-cooled boiling on nano-structured surface. *Int. J. Heat Mass Transf.* **2016**, *100*, 276–286. [CrossRef]
25. Li, X.; Cole, I.; Tu, J. A review of nucleate boiling on nanoengineered surfaces—The nanostructures, phenomena and mechanisms. *Int. J. Heat Mass Transf.* **2019**, *141*, 20–33. [CrossRef]
26. Wu, N.; Zeng, L.; Fu, T.; Wang, Z.; Lu, C. Molecular dynamics study of rapid boiling of thin liquid water film on smooth copper surface under different wettability conditions. *Int. J. Heat Mass Transf.* **2020**, *147*, 118905.1–118905.5. [CrossRef]
27. Cao, Q.; Shao, W.; Ren, X.; Ma, X.; Shao, K.; Cui, Z.; Liu, Y. Molecular dynamics simulations of the liquid film evaporation heat transfer on different wettability hybrid surfaces at the nanoscale. *J. Mol. Liq.* **2020**, *314*, 113610. [CrossRef]
28. Liang, Z.; Chandra, A.; Bird, E.; Keblinski, P. A molecular dynamics study of transient evaporation and condensation. *Int. J. Heat Mass Transf.* **2020**, *149*, 119152. [CrossRef]
29. Carey, V.P.; Wemhoff, A.P. Thermodynamic analysis of near-wall effects on phase stability and homogeneous nucleation during rapid surface heating. *Int. J. Heat Mass Transf.* **2005**, *48*, 5431–5445. [CrossRef]
30. Shen, B.; Yamada, M.; Mine, T.; Hidaka, S.; Kohno, M.; Takahashi, K.; Takata, Y. Depinning of bubble contact line on a biphilic surface in subatmospheric boiling: Revisiting the theories of bubble departure. *Int. J. Heat Mass Transf.* **2018**, *126 Pt B*, 715–720. [CrossRef]
31. Meloni, S.; Giacomello, A.; Casciola, C.M. Focus Article: Theoretical aspects of vapor/gas nucleation at structured surfaces. *J. Chem. Phys.* **2016**, *145*, 211802. [CrossRef]
32. Verlet, L. Computer "Experiments" on Classical Fluids. I. Thermodynamical Properties of Lennard-Jones Molecules. *Phys. Rev.* **1967**, *159*, 98–103. [CrossRef]